

SHARM: Segmented Head Anatomical Reference Models

Essam A. Rashed^a, Mohammad Al-Shatouri^b, Ilkka Laakso^{c,d}, Akimasa Hirata^{e,f}

^aGraduate School of Information Science, University of Hyogo, Kobe 650-0047, Japan

^bRadiology Department, Faculty of Medicine, Suez Canal University, Ismailia 41522, Egypt

^cDepartment of Electrical Engineering and Automation, Aalto University, Espoo, Finland

^dAalto neuroimaging, Aalto University, Espoo, Finland

^eDepartment of Electrical and Mechanical Engineering, Nagoya Institute of Technology, Nagoya 466-8555, Japan

^fCenter of Biomedical Physics and Information Technology, Nagoya Institute of Technology, Nagoya 466-8555, Japan

Abstract

Reliable segmentation of anatomical tissues of human head is a major step in several clinical applications such as brain mapping, surgery planning and associated computational simulation studies. Segmentation is based on identifying different anatomical structures through labeling different tissues through medical imaging modalities. The segmentation of brain structures is commonly feasible with several remarkable contributions mainly for medical perspective; however, non-brain tissues are of less interest due to anatomical complexity and difficulties to be observed using standard medical imaging protocols. The lack of whole head segmentation methods and unavailability of large human head segmented datasets limiting the variability studies, especially in the computational evaluation of electrical brain stimulation (neuromodulation), human protection from electromagnetic field, and electroencephalography where non-brain tissues are of great importance.

To fill this gap, this study provides an open-access Segmented Head Anatomical Reference Models (SHARM) that consists of 196 subjects. These models are segmented into 15 different tissues; skin, fat, muscle, skull cancellous bone, skull

Email address: rashed@sis.u-hyogo.ac.jp (Essam A. Rashed)

cortical bone, brain white matter, brain gray matter, cerebellum white matter, cerebellum gray matter, cerebrospinal fluid, dura, vitreous humor, lens, mucous tissue and blood vessels. The segmented head models are generated using open-access IXI MRI dataset through convolutional neural network structure named ForkNet⁺. Results indicate a high consistency in statistical characteristics of different tissue distribution in age scale with real measurements. SHARM is expected to be a useful benchmark not only for electromagnetic dosimetry studies but also for different human head segmentation applications.

Keywords: Human head models, brain segmentation, convolutional neural networks, MRI

1. Introduction

Anatomical reference models of human subjects are of great importance in several computer simulation studies such as medical imaging, dosimetric evaluation for diagnosis and therapy and human safety. In principle, digital models are generated from anatomical imaging of real subjects for better understanding real physical effects. Specifically, personalized electrode positions or coil location are explored in the non-invasive electrical and magnetic stimulation ([Antonenko et al., 2019](#)), in addition to group-level optimization([Gomez-Tames et al., 2018](#); [Laakso et al., 2015](#)). Variability analysis is needed to derive the limit in human protection from electromagnetic field ([Hirata et al., 2021](#); [ICNIRP et al., 2020](#)).

Several attempts provided different models that represent whole body models ([Christ et al., 2009](#); [Kim et al., 2008](#); [Nagaoka et al., 2004](#); [Segars et al., 2010](#); [Yu et al., 2015](#)). A useful review is in ([Kainz et al., 2019](#)). Segmentation of brain tissues is of high interest in several clinical applications such as diagnosis of abnormalities, assessment of neurophysiological performance, surgery planing and many others. Most of standard medical imaging applications can represent brain tissues in high contrast which enable accurate automatic annotation ([Baur et al., 2021](#)). However, segmentation of non-brain tissues is challenging as it represented in low contrast and/or allocated in limited regions.

Moreover, in clinical medical applications, imaging protocols are usually adjusted such that brain tissues are presented in high quality as the main target of diagnostic applications (Kalavathi and Prasath, 2016).

Whole head segmentation have been discussed mainly for the development of digital models for electromagnetic stimulation studies. SimNibs is an open source software for the simulation of non-invasive brain stimulation that include magnetic resonance (MR) image segmentation to generate head models (Saturnino et al., 2018; Thielscher et al., 2015). However, segmentation is limited to major head tissues such as white matter (WM), grey matter (GM), cerebrospinal fluid (CSF), skull and scalp. ROAST is another pipeline the include automatic MRI segmentation based on SPM12 (Ashburner and Friston, 2005) with variety of segmentation and electromagnetic modeling options (Huang et al., 2019). However, ROAST segmentation is also limited to a few number of tissues as in Table 1 in Ref. (Huang et al., 2019). Segmentation of fifteen head tissues using multi-modality images (MRI T1/T2, mDixon, venogram and CT) is proposed in (Puonti et al., 2020). Recently, the use of deep learning architectures demonstrate quality improvement of anatomical segmentation (Akkus et al., 2017). Several network architectures such as ForkNet (Rashed et al., 2019), SubForkNet (Rashed et al., 2020) and FastSurfer (Henschel et al., 2020) have been used to generate human head models with different scope and applications.

Due to the complexity of full head segmentation and requirements of intensive efforts for manual parameters adjustment, there is a shortage of relatively large dataset of human head models. This problem becomes more feasible with the use of deep learning as robust segmentation tool with superior accuracy compared to conventional methods. The aim of this work is to generate an open-access Segmented Head Anatomical Reference Models (SHARM) that is large enough for subject variability studies. The developed dataset consists of 196 subjects segmented into 15 different tissues. The main contributions of this study can be summarized as follows:

- An open-source deep learning pipeline for automatic segmentation of MRI

head images.

- An open-access large human head dataset segmented into brain and non-brain tissues.
- Evaluation of the consistency of segmented models with realistic tissue characteristics.

2. Materials and methods

2.1. Dataset and general pipeline

The MRI dataset used in this study is the IXI Dataset¹ which consists of around 600 MRI scans of healthy subjects. A set of 196 subjects are selected (123 females, 70 males, and 3 unknown), that are imaged at two hospitals (100 were imaged at the Guy’s Hospital (London, UK) with Philips 1.5T system and 96 were imaged at the Hammersmith Hospital (London, UK) using a Philips 3T system). Excluded images criteria are based on quality of the image and availability of multi-modality scans. The T1w/T2w image data are in Nifti formats and are used for generation of the head models.

The raw T1 and T2-weighted MR images are registered using non-rigid registration such that T2w are adjusted to fit with T1w. The acoustic noise is reduced through contouring of head surface and relabeling external region as air voxels. The N4 bias field correction method (ITK²) is used for bias correction of both MRI modalities. Both T1w/T2w images are normalized with zero mean and unit variance, then scaled to values [0.01, 0.99]. All the above pre-processing procedures are used to generate the network input volumes (a set of two 256³ volumes representing T1w/T2w MRI with unified 1³mm resolution). A selected set of the network input is segmented into 15 different head tissues using the semi-automatic method detailed in (Laakso et al., 2015). The segmentation binary labels are used as network target (output) through training process. The

¹<http://brain-development.org/ixi-dataset/>

²<https://itk.org/>

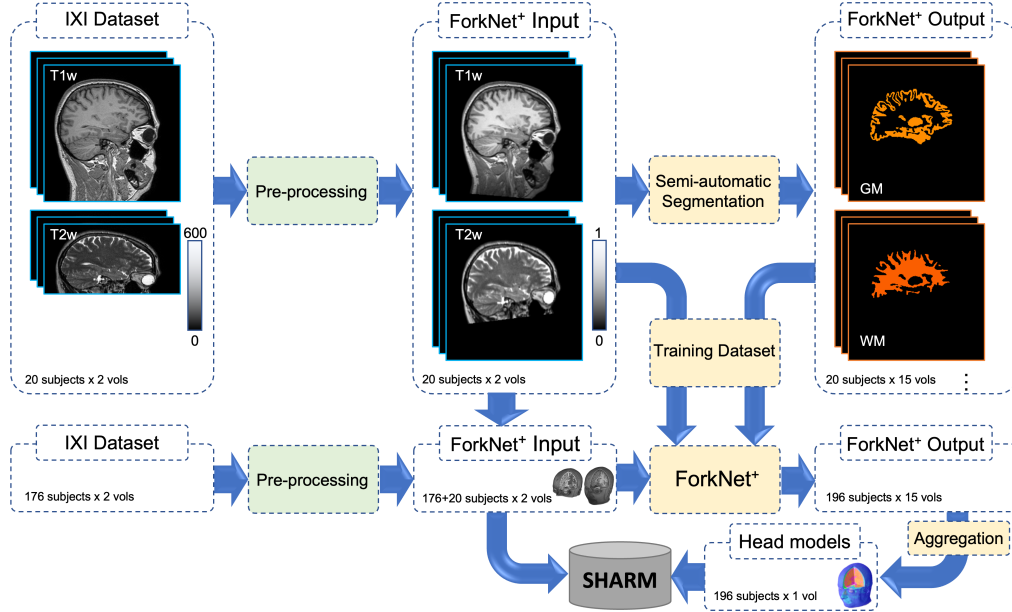


Figure 1: Data flow used to generate SHARM from IXI dataset.

remaining subjects are evaluated using trained network to automatically generate segmentation labels. Finally, an aggregation process is used to combine different segmentation labels into a head model. The pre-processed MR scans and segmented head models are available for each subject in SHARM dataset. The data processing pipeline is shown in Fig. 1.

2.2. Semi-automatic segmentation

The target dataset for the training process was generated using a semi-automatic segmentation pipeline that segments T1- and T2-weighted MR image data into 15 tissue types (Laakso et al., 2015). Briefly, after bias correction and normalization of the MR data, the pipeline first splits the head into three compartments: inner compartment, consisting of the volume inside the inner surface of the skull; middle compartment, consisting of the skull and nasal cavity; and the outer compartment, consisting of the volume between the outer surface of the skull and the outer surface of the skin. The quality of these

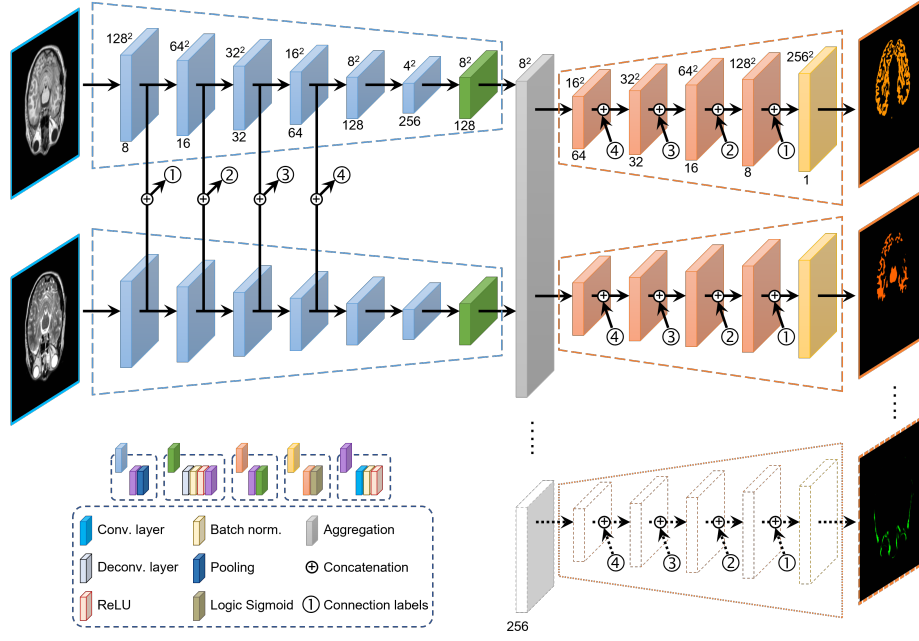


Figure 2: ForkNet⁺ with MRI T1w/T2w inputs and N segmented tissues outputs.

compartments is verified by visual inspection, and whenever necessary, control parameters are manually altered until the compartments match the MR data.

The inner compartment is segmented into brain using FreeSurfer image analysis software (Dale et al., 1999; Fischl and Dale, 2000). The brain segmentation consists of cerebral gray matter, cerebral white matter, cerebellar gray matter, cerebellar white matter, deep brain structures (brainstem, accumbens, amygdala, caudate, hippocampus, pallidum, putamen, thalamus), and ventricular CSF. The remaining non-brain volume in the inner compartment is segmented into CSF (bright T2-weighted image), blood (dark T2), and dura (non-brain non-CSF tissue close to the inner boundary of the skull). Anterior and middle cerebral arteries initially estimated from T2 are corrected using thresholding of registered MRA images (when available). Deep brain structures are treated as GM. The middle compartment consisting of the skull is segmented into cortical and cancellous bone by thresholding the T2-weighted MRI data. It is ensured

that the inner and outer cortical bone layers are at least 1 mm and 1.5 mm thick, respectively. The nasal cavity also belongs to the middle compartment and is segmented as either mucous tissue or cortical bone based on T2-weighted images. The outer compartment is segmented into skin, fat, muscle, and eyes. The scalp (including subcutaneous fat) is segmented as the outer layer of the head, with thickness between 2 mm and 10 mm. Fat and muscle are segmented based on thresholding the T1-weighted image data. Finally, eyes and lens are segmented using both T1- and T2-weighted image data.

The resulting segmentation has uniform voxel size of $0.5\text{ mm} \times 0.5\text{ mm} \times 0.5\text{ mm}$, half of that of the input MR images. In this study, the segmented dataset was downsampled to the same resolution as the input images using three-dimensional nearest neighborhood interpolation algorithm.

2.3. Network architecture

The deep learning architecture used here is an extension of ForkNet ([Rashed et al., 2019](#)) by considering input data from both T1- and T2-weighted MRI scans. We then refer to the new network as ForkNet⁺. The network inputs are the MRI scans in two encoders and outputs are N decoders each assigned to single anatomical structure (here $N=15$). The details of the layer structures and data processing flow is shown in Fig. 2. The network output are binary masks that identify different anatomical tissues/liquids such as skin, muscle, fat, skull (cortical bone), skull (cancellous bone), CSF, blood vessels, dura, brain GM, brain WM, cerebellum GM, cerebellum WM, vitreous humor, eye lens, mucous tissue and whole head. ForkNet⁺ design is flexible and easy to be adjusted to segmented specific number of tissues for different applications as each tissue is segmented using separate decoder (Fig. 2).

2.4. Head model generation

Once the network is well-trained, the head models are generated through fast evaluation process. To reduce artifacts caused by 2D slice segmentation, a set of three networks are trained using slices of axial, sagittal and coronal

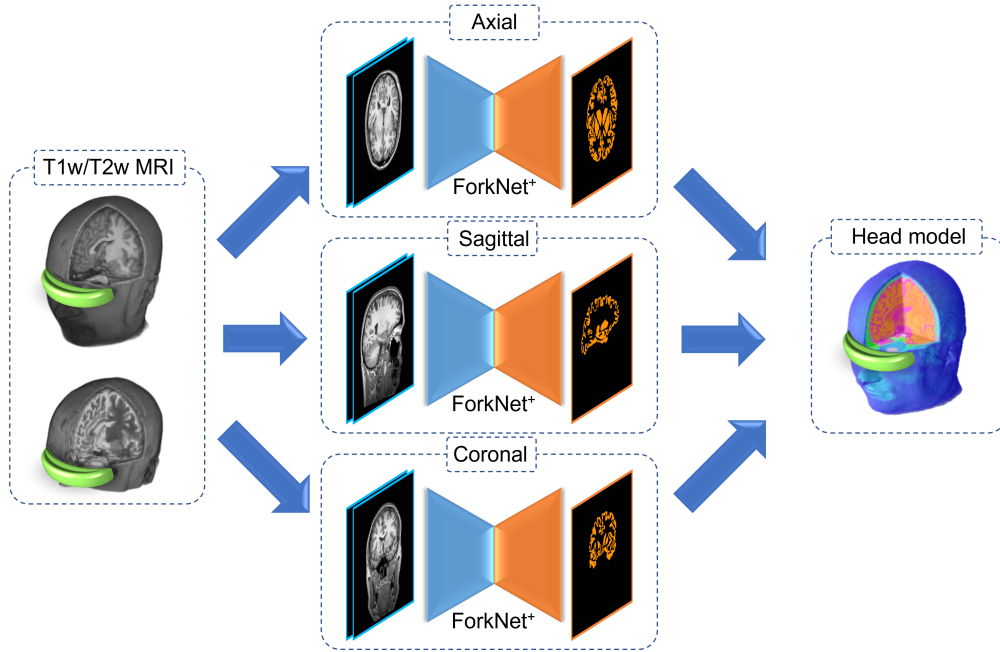


Figure 3: Network evaluation through different direction to generate the head model.

directions as shown in Fig. 3. A rule-based segmentation merge approach using majority vote is used to generate the final segmentation from different slicing directions. When no majority in a voxel is found, the neighborhood majority vote (Rashed et al., 2020).

3. Results

A set of 20 randomly selected head models and associated segmented labels are used to train ForkNet⁺. The network architecture is developed using Wolfram Mathematica (R) ver. 13.0, installed on a Ubuntu 20.04 workstation of 12 Cores Intel (R) Core (TM) i9-10920X @3.50GHz, 64 GB memory, and NVIDIA RTX A6000 GPU. A three networks (axial, sagittal and coronal) are trained with cross-entropy loss function and ADAM optimization algorithm. The training was considered using 50 epochs with batch size 4. To reduce the computation cost, the number of output tracks is set to $N = 4$ (i.e., a set of 4

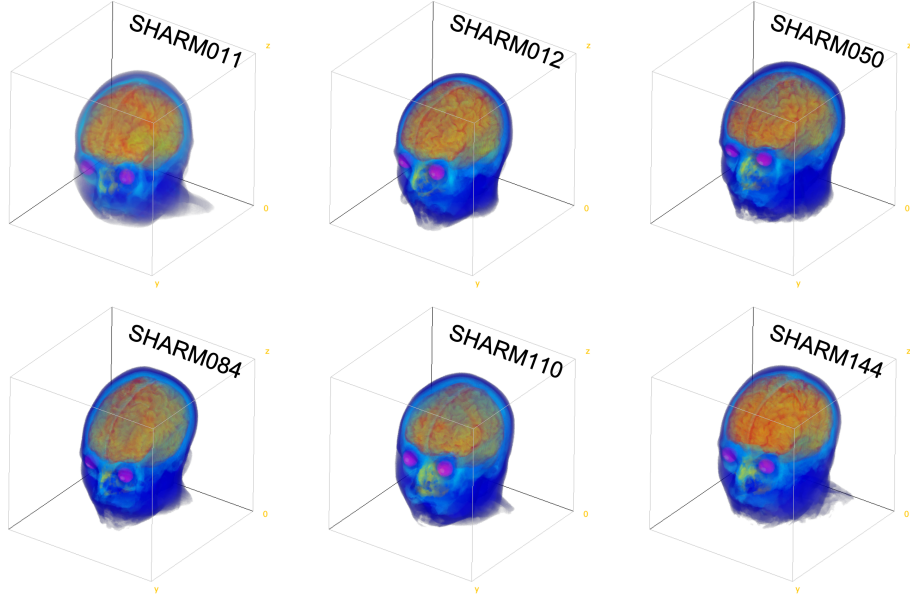


Figure 4: Volume rendering sample of generated head models.

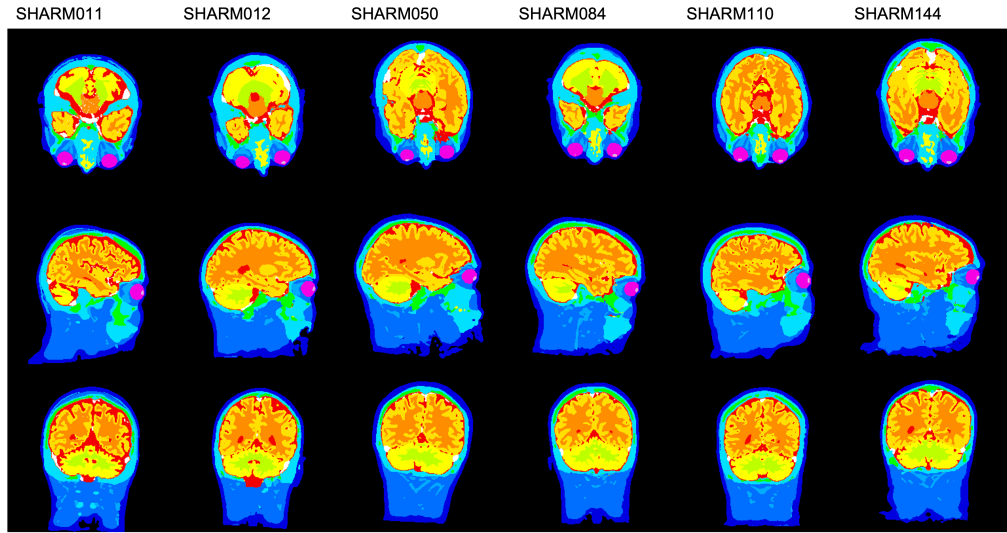


Figure 5: Axial, sagittal and coronal slices (top to bottom) of head models shown in Fig. 4 in order.

tissues are trained simultaneously). A single training round requires about 24 mins.

The remaining 176 head models are evaluated through trained networks and the network output is aggregated to generate the head models. Example of generated head models are shown in Figs. 4 and 5. In some few cases, some manual edition is required mainly to remove a small regions of CSF-like tissue uncorrected segmented inside the mouth. Some other cases are excluded due to the strong noise that is difficult to be automatically removed and lead to incorrect segmentation of external contour. Evaluation of segmentation accuracy is not conducted due to the lack of manual true annotation and it is out of the scope of this work. However, we provide quantitative assessment of different tissues of the SHARM dataset. In principle, we study the variability of segmented volumes within age scale to validate the validity of SHARM models.

Figure 6 demonstrates a regression curves of segmented brains. Brain is considered as a composition of GM, WM and CSF. It shows that a decline in global GM volume with age ($R^2=0.274$), while there is no significant change in WM volume with age ($R^2=0.001$). A remarkable increase in CSF volume with age ($R^2=0.277$). Difference between gender grouping and percentage of different structures with respect to total intracranial volume (TIV) are also shown in Fig. 6 and it is consistent with results reported in literature (e.g., (Ge et al., 2002; Good et al., 2001; Ruigrok et al., 2014)). The change in TIV over age and the correlation between GM/WM ratio with age is shown in Fig. 7. The change of skin, muscle, fat, skull, vitreous humor, and eye lens volumes is shown in Fig. 8. In general the volume of skin, muscles, and fat tissues are increasing with aging. Skull and eye lens does not change so much while the volume of vitreous humor is shrinked as reported earlier (Sebag, 1987). Data shown in Fig. 9 demonstrate that the volume of brain is highly correlated with the body mass index (BMI) and brain volume of male subjects are of large volume compared with females (Eliot et al., 2021). SHARM dataset can be

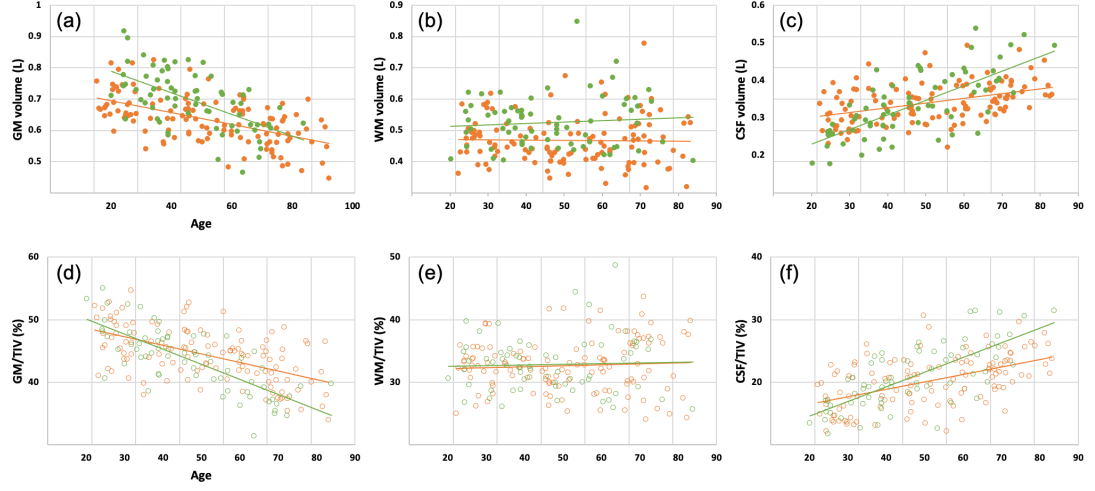


Figure 6: (a) Regression lines with scatter plot of total GM volume over age for all subjects (female in orange and male in green). (b) and (c) are regression lines and scatter plots for total WM and CSF, respectively. (d)-(f) are the regression lines and scatter plots for fractional volume (with respect to TIV) of GM, WM and CSF, respectively.

download³ in MATLAB (*.mat) files with structure shown in Fig. 10.

4. Discussion

This work demonstrate a new benchmark dataset for several computational neuroscience applications. The open-access SHARM consists of 196 head models segmented into 15 different tissues that cover a wide range of subject variability. A boxplot demonstrates the volume variations of different structures in SHARM is shown in Fig. 11. It is clearly observed that skull volume is 0.827 ± 0.08 L (male) and 0.730 ± 0.08 L (female). These values are highly correlated with those listed in the ICRP Reference man (averaged bone without marrow of Skull is 708 gm). The vitreous humor is 15.098 ± 2.10 mL (male) and 14.124 ± 1.91 mL (female) that is referenced as value 15 ± 6.5 gm in adult (ICRP Publication 23, 1975, Table 97, p. 220). Also, eye lens is 0.246 ± 0.07 mL

³<https://figshare.com/s/a4d9ba6f18a6b7f7ba2c> (zip, 7.62 GB)

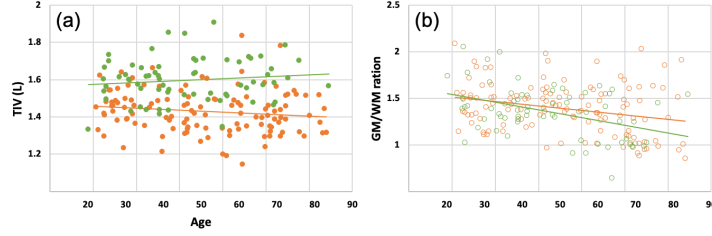


Figure 7: (a) Regression curves and scatter plot of (a) total intracranial volume (TIV) in liters and (b) GM/WM ratio over age for all subjects.

Table 1: Comparison of volume/weight values of SHARM models with ICRP Reference man (ICRP Publication 23, 1975).

#	Tissue	Density*	Gender	Volume (mL)		Weight (gm)		Reference value	Comments**
				Mean	SD	Mean	SD		
1	Brain (GM+WM+CSF)	1,041	M	1,437	105	1,503	110	1,355 gm	Adult (20-60 y), Table 93
			F	1,277	108	1,336	113	1200 gm	
2	Cerebellum	1,045	M	124	14	130	14	100 ~ 133 gm	Adult (20-90 y), Eq @ p.212
			F	115	15	120	16		
3	Vitreous humor	1,005	M	15.1	2.11	15.172	2.1	15±6.5 gm	Table 97
			F	14.1	1.91	14.19	1.9		
4	Eye lens	1,076	M	0.246	0.07	0.264	0.075	172 ~ 258 mg	Table 100
			F	0.242	0.08	0.26	0.086		
5	Skull	1,908	M	827	79	1,578	151	706 gm	Table 16
			F	730	82	1,393	156		

* Average density values are acquired from (IT's Foundation, 2023)

** References from (ICRP Publication 23, 1975)

(male) and 0.242 ± 0.08 mL (female) which is calculated as 172 to 258.1 gm for (20 - 60 y) adult (ICRP Publication 23, 1975, Table 100, p. 225). Calculated volume and weight of different SHARM tissues are compared with those reported in (ICRP Publication 23, 1975) in Table 1. These values are example that indicate segmentation accuracy of non-brain tissues.

The segmented models along with normalized T1- and T2-weighted MR scans are available for each subject in addition to other demographic information. Most of the models in SHARM are presented with full head and neck segmentation which enables simulation studies that requires full head models. moreover, the trained deep learning model used to generate SHARM is shared which can be used to generate additional models considering the availability of consistent MR scans. The software ForkNet⁺ generate individual tissue segmen-

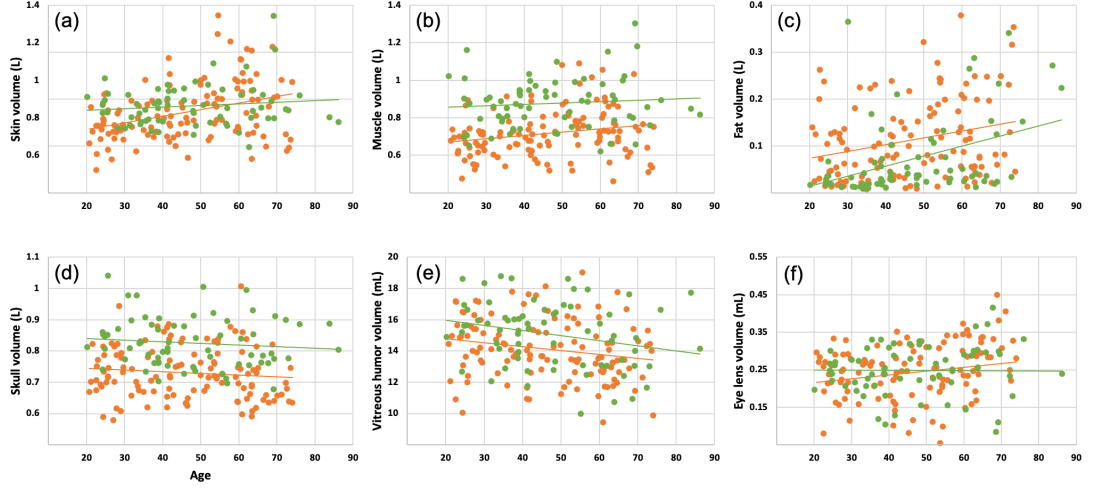


Figure 8: Regression curves of segmented volume of (a) skin, (b) muscle, (c) fat, (d) skull, (e) vitreous humor, and (f) eye lens in SHARM models.

tation in terms of probability maps which enables customized segmentation of a single subject through weighting based aggregation process (similar to those presented in (Rashed et al., 2021)). It is worth noting that evaluation of segmentation accuracy is out of the scope of this work, because earlier version of the ForkNet (Rashed et al., 2019) segmentation have been evaluated.

The limitation of this work is the lack of variability of MR data acquisition. Data are acquired from two scanners installed at two medical institutes but it is developed by the same manufacturer. Further extension with data from other manufacturers are planned to be included in future versions. Moreover, we will include more information considering the segmentation of deep brain structures and fiber orientations in future versions of SHARM. Also, there is a lack of bone structure accuracy in the neck region as lack of neck data in T2 images. In future, we will investigate potential approaches to improve the segmentation neck region properly.

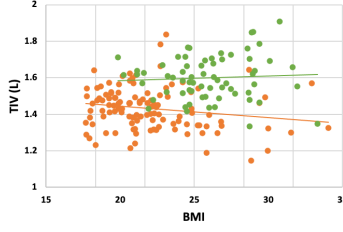


Figure 9: Regression curves of TIV per BMI.

5. Conclusion

In this study, we present SHARM, a benchmark dataset of 196 segmented human head models. The models are segmented into 15 different tissues using deep learning network named ForkNet⁺. The freely available models along with normalized MR T1- and T2-weighted scans would enable a large scale studies in different applications such as electromagnetic brain stimulations. Results demonstrate that the segmented models are of high consistency with measurements obtained from real measurements. One feature of ForkNet⁺ is the segmentation of each tissue is generated as probability maps that enable parametric segmentation for further customization of the generated head models. The trained networks as well as source code are shared for potential usage of head models generation. With large scale of subject age, SHARM would enable different electromagnetic dosimetry and human safety studies in a reliable manner. After publication, Mathematica notebooks demonstrate the implementation of ForkNet⁺ architectures and trained networks will be available for download at: <https://github.com/erashed/ForkNetPlus>

Acknowledgment

This work was funded by the Japan Society for the Promotion of Science (JSPS), a Grant-in-Aid for Scientific Research, Grant number JSPS KAKENHI 22K12765.

```

ID: 'SHARM076'
model: [256×256×256 uint8]
T1w: [256×256×256 double]
T2w: [256×256×256 double]
size: [256 256 256]
resolution: [1 1 1]
mf: '1.5T'
gender: 'female'
age: 36.0600
height: 163
weight: 64
reference: 'IXI222'
comments: 'N/A'
version: '1.1'
date: '15 Nov. 2022'

```

Figure 10: Structure of subject SHARM076 that include MRI scans, head model and other subject details.

References

- Akkus, Z., Galimzianova, A., Hoogi, A., Rubin, D.L., Erickson, B.J., 2017. Deep learning for brain MRI segmentation: state of the art and future directions. *Journal of digital imaging* 30, 449–459. doi:[10.1007/s10278-017-9983-4](https://doi.org/10.1007/s10278-017-9983-4).
- Antonenko, D., Thielscher, A., Saturnino, G.B., Aydin, S., Ittermann, B., Grittnet, U., Flöel, A., 2019. Towards precise brain stimulation: Is electric field simulation related to neuromodulation? *Brain Stimulation* 12, 1159–1168. doi:[10.1016/j.brs.2019.03.072](https://doi.org/10.1016/j.brs.2019.03.072).
- Ashburner, J., Friston, K.J., 2005. Unified segmentation. *NeuroImage* 26, 839–851. doi:[10.1016/j.neuroimage.2005.02.018](https://doi.org/10.1016/j.neuroimage.2005.02.018).
- Baur, C., Denner, S., Wiestler, B., Navab, N., Albarqouni, S., 2021. Autoencoders for unsupervised anomaly segmentation in brain mr images: A comparative study. *Medical Image Analysis* 69, 101952. doi:[10.1016/j.media.2020.101952](https://doi.org/10.1016/j.media.2020.101952).
- Christ, A., Kainz, W., Hahn, E.G., Honegger, K., Zefferer, M., Neufeld, E., Rascher, W., Janka, R., Bautz, W., Chen, J., Kiefer, B., Schmitt, P., Hollenbach, H.P., Shen, J., Oberle, M., Szczerba, D., Kam, A., Guag, J.W.,

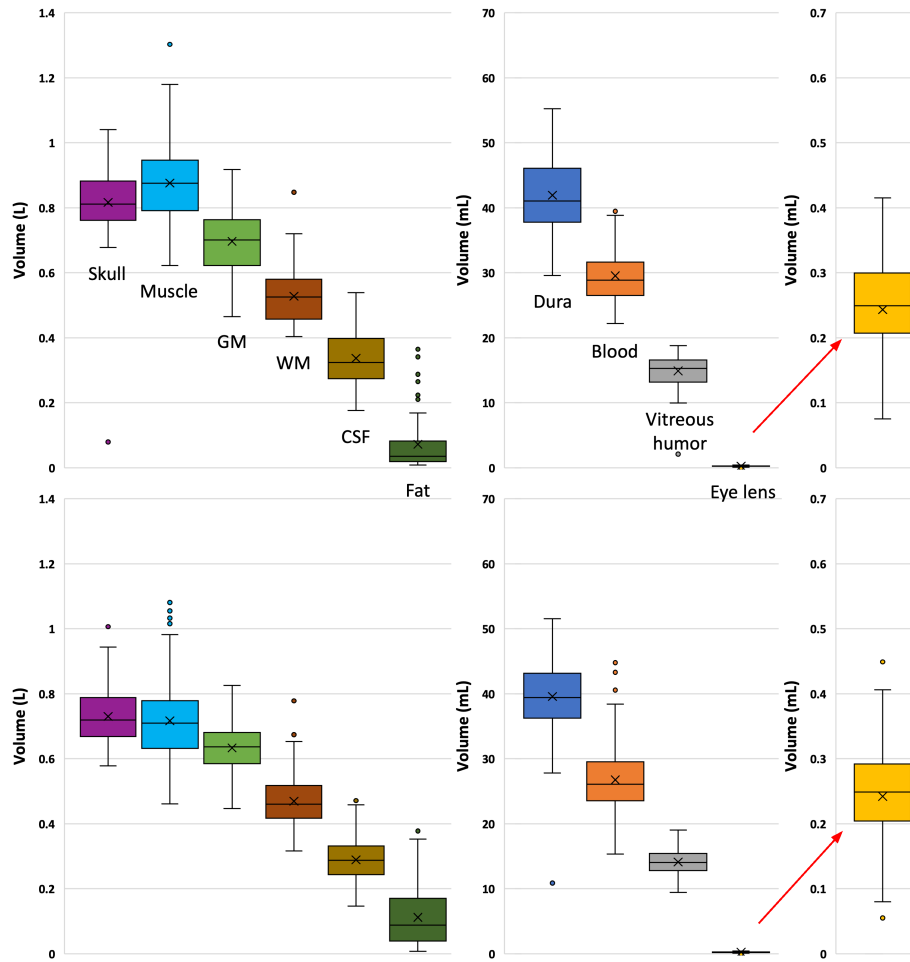


Figure 11: Boxplot demonstrates volume variations of different structures in SHARM male (top) and female (bottom) subjects.

- Kuster, N., 2009. The Virtual Family—development of surface-based anatomical models of two adults and two children for dosimetric simulations. *Physics in Medicine and Biology* 55, N23–N38. doi:[10.1088/0031-9155/55/2/n01](https://doi.org/10.1088/0031-9155/55/2/n01).
- Dale, A.M., Fischl, B., Sereno, M.I., 1999. Cortical surface-based analysis: I. segmentation and surface reconstruction. *NeuroImage* 9, 179–194. doi:[10.1006/nimg.1998.0395](https://doi.org/10.1006/nimg.1998.0395).
- Eliot, L., Ahmed, A., Khan, H., Patel, J., 2021. Dump the “dimorphism”: Comprehensive synthesis of human brain studies reveals few male-female differences beyond size. *Neuroscience & Biobehavioral Reviews* 125, 667–697. doi:[10.1016/j.neubiorev.2021.02.026](https://doi.org/10.1016/j.neubiorev.2021.02.026).
- Fischl, B., Dale, A.M., 2000. Measuring the thickness of the human cerebral cortex from magnetic resonance images. *Proceedings of the National Academy of Sciences* 97, 11050–11055. doi:[10.1073/pnas.200033797](https://doi.org/10.1073/pnas.200033797).
- Ge, Y., Grossman, R.I., Babb, J.S., Rabin, M.L., Mannon, L.J., Kolson, D.L., 2002. Age-related total gray matter and white matter changes in normal adult brain. Part I: volumetric MR imaging analysis. *American Journal of Neuroradiology* 23, 1327–1333. URL: <http://www.ajnr.org/content/23/8/1327>.
- Gomez-Tames, J., Hamasaka, A., Laakso, I., Hirata, A., Ugawa, Y., 2018. Atlas of optimal coil orientation and position for tms: A computational study. *Brain Stimulation* 11, 839–848. doi:[10.1016/j.brs.2018.04.011](https://doi.org/10.1016/j.brs.2018.04.011).
- Good, C.D., Johnsrude, I.S., Ashburner, J., Henson, R.N., Friston, K.J., Frackowiak, R.S., 2001. A voxel-based morphometric study of ageing in 465 normal adult human brains. *NeuroImage* 14, 21–36. doi:[10.1006/nimg.2001.0786](https://doi.org/10.1006/nimg.2001.0786).
- Henschel, L., Conjeti, S., Estrada, S., Diers, K., Fischl, B., Reuter, M., 2020. FastSurfer - a fast and accurate deep learning based neuroimaging pipeline. *NeuroImage* 219, 117012. doi:[10.1016/j.neuroimage.2020.117012](https://doi.org/10.1016/j.neuroimage.2020.117012).

- Hirata, A., Diao, Y., Onishi, T., Sasaki, K., Ahn, S., Colombi, D., De Santis, V., Laakso, I., Giaccone, L., Joseph, W., Rashed, E.A., Kainz, W., Chen, J., 2021. Assessment of human exposure to electromagnetic fields: Review and future directions. *IEEE Transactions on Electromagnetic Compatibility* 63, 1619–1630. doi:[10.1109/TEM.2021.3109249](https://doi.org/10.1109/TEM.2021.3109249).
- Huang, Y., Datta, A., Bikson, M., Parra, L.C., 2019. Realistic volumetric approach to simulate transcranial electric stimulation—ROAST—a fully automated open-source pipeline. *Journal of Neural Engineering* 16, 056006. doi:[10.1088/1741-2552/ab208d](https://doi.org/10.1088/1741-2552/ab208d).
- ICNIRP, et al., 2020. Gaps in knowledge relevant to the “guidelines for limiting exposure to time-varying electric and magnetic fields (1 Hz–100 kHz)”. *Health physics* 118, 533–542. doi:[10.1097/HP.0000000000001261](https://doi.org/10.1097/HP.0000000000001261).
- ICRP Publication 23, 1975. Reference Man: Anatomical, Physiological and Metabolic Characteristics (Annals of the ICRP). Pergamon Press, Oxford. URL: http://journals.sagepub.com/pb-assets/cmscontent/ANI/P_023_1975_Report_on_the_Task_Group_on_Reference_Man_rev0.pdf.
- IT’s Foundation, 2023. Human body density values. <https://itis.swiss/virtual-population/tissue-properties/database/density/>. [Online; accessed 10-Sept-2023].
- Kainz, W., Neufeld, E., Bolch, W.E., Graff, C.G., Kim, C.H., Kuster, N., Lloyd, B., Morrison, T., Segars, P., Yeom, Y.S., Zankl, M., Xu, X.G., Tsui, B.M.W., 2019. Advances in computational human phantoms and their applications in biomedical engineering—a topical review. *IEEE Transactions on Radiation and Plasma Medical Sciences* 3, 1–23. doi:[10.1109/TRPMS.2018.2883437](https://doi.org/10.1109/TRPMS.2018.2883437).
- Kalavathi, P., Prasath, V.S., 2016. Methods on skull stripping of MRI head scan images—a review. *Journal of digital imaging* 29, 365–379. doi:[10.1007/s10278-015-9847-8](https://doi.org/10.1007/s10278-015-9847-8).

- Kim, C.H., Choi, S.H., Jeong, J.H., Lee, C., Chung, M.S., 2008. HDRK-man: a whole-body voxel model based on high-resolution color slice images of a korean adult male cadaver. *Physics in Medicine and Biology* 53, 4093–4106. doi:[10.1088/0031-9155/53/15/006](https://doi.org/10.1088/0031-9155/53/15/006).
- Laakso, I., Tanaka, S., Koyama, S., De Santis, V., Hirata, A., 2015. Inter-subject variability in electric fields of motor cortical tDCS. *Brain Stimulation* 8, 906–913. doi:[10.1016/j.brs.2015.05.002](https://doi.org/10.1016/j.brs.2015.05.002).
- Nagaoka, T., Watanabe, S., Sakurai, K., Kunieda, E., Watanabe, S., Taki, M., Yamanaka, Y., 2004. Development of realistic high-resolution whole-body voxel models of Japanese adult males and females of average height and weight, and application of models to radio-frequency electromagnetic-field dosimetry. *Physics in Medicine and Biology* 49, 1–15. doi:[10.1088/0031-9155/49/1/001](https://doi.org/10.1088/0031-9155/49/1/001).
- Puonti, O., Van Leemput, K., Saturnino, G.B., Siebner, H.R., Madsen, K.H., Thielscher, A., 2020. Accurate and robust whole-head segmentation from magnetic resonance images for individualized head modeling. *NeuroImage* 219, 117044. doi:[10.1016/j.neuroimage.2020.117044](https://doi.org/10.1016/j.neuroimage.2020.117044).
- Rashed, E.A., Gomez-Tames, J., Hirata, A., 2019. Development of accurate human head models for personalized electromagnetic dosimetry using deep learning. *NeuroImage* 202, 116132. doi:[10.1016/j.neuroimage.2019.116132](https://doi.org/10.1016/j.neuroimage.2019.116132).
- Rashed, E.A., Gomez-Tames, J., Hirata, A., 2020. End-to-end semantic segmentation of personalized deep brain structures for non-invasive brain stimulation. *Neural Networks* 125, 233–244. doi:[10.1016/j.neunet.2020.02.006](https://doi.org/10.1016/j.neunet.2020.02.006).
- Rashed, E.A., Gomez-Tames, J., Hirata, A., 2021. Influence of segmentation accuracy in structural MR head scans on electric field computation for TMS and tES. *Physics in Medicine and Biology* 66, 064002. doi:[10.1088/1361-6560/abe223](https://doi.org/10.1088/1361-6560/abe223).

- Ruigrok, A.N., Salimi-Khorshidi, G., Lai, M.C., Baron-Cohen, S., Lombardo, M.V., Tait, R.J., Suckling, J., 2014. A meta-analysis of sex differences in human brain structure. *Neuroscience & Biobehavioral Reviews* 39, 34–50. doi:[10.1016/j.neubiorev.2013.12.004](https://doi.org/10.1016/j.neubiorev.2013.12.004).
- Saturnino, G.B., Puonti, O., Nielsen, J.D., Antonenko, D., Madsen, K.H., Thielscher, A., 2018. Simnibs 2.1: A comprehensive pipeline for individualized electric field modelling for transcranial brain stimulation. *bioRxiv* doi:[10.1101/500314](https://doi.org/10.1101/500314).
- Sebag, J., 1987. Ageing of the vitreous. *Eye* 1, 254–262.
- Segars, W.P., Sturgeon, G., Mendonca, S., Grimes, J., Tsui, B.M.W., 2010. 4D XCAT phantom for multimodality imaging research. *Medical Physics* 37, 4902–4915. doi:[10.1118/1.3480985](https://doi.org/10.1118/1.3480985).
- Thielscher, A., Antunes, A., Saturnino, G.B., 2015. Field modeling for transcranial magnetic stimulation: A useful tool to understand the physiological effects of TMS?, in: 2015 37th Annual International Conference of the IEEE Engineering in Medicine and Biology Society (EMBC), pp. 222–225. doi:[10.1109/EMBC.2015.7318340](https://doi.org/10.1109/EMBC.2015.7318340).
- Yu, D., Wang, M., Liu, Q., 2015. Development of chinese reference man deformable surface phantom and its application to the influence of physique on electromagnetic dosimetry. *Physics in Medicine and Biology* 60, 6833–6846. doi:[10.1088/0031-9155/60/17/6833](https://doi.org/10.1088/0031-9155/60/17/6833).